nature immunology

Structural evidence for a germline-encoded T cell receptor–major histocompatibility complex interaction 'codon'

Dan Feng[1], Christopher J Bond[1], Lauren K Ely[1], Jennifer Maynard[1,2] & K Christopher Garcia[1]

All complexes of T cell receptors (TCRs) bound to peptide–major histocompatibility complex (pMHC) molecules assume a stereotyped binding 'polarity', despite wide variations in TCR-pMHC docking angles. However, existing TCR-pMHC crystal structures have failed to show broadly conserved pairwise interaction motifs. Here we determined the crystal structures of two TCRs encoded by the variable β-chain 8.2 (V_β8.2), each bound to the MHC class II molecule I-A^u, and did energetic mapping of V_α and V_β contacts with I-A^u. Together with two previously solved structures of V_β8.2-containing TCR-MHC complexes, we found four TCR–I-A complexes with structurally superimposable interactions between the V_β loops and the I-A α-helix. This examination of a narrow 'slice' of the TCR-MHC repertoire demonstrates what is probably one of many germline-derived TCR-MHC interaction 'codons'.

The antigen-specific T cell–mediated immune response is initiated by the productive interaction of an αβ T cell receptor (TCR) with a major histocompatibility complex (MHC) molecule presenting a processed peptide. The importance of this interaction in cellular immunity has spurred great interest in elucidating, through analysis of crystal structures of αβTCR molecules bound to peptide-MHC (pMHC) complexes, the molecular principles governing 'MHC restriction'. Studies of approximately 17 unique TCR-pMHC complexes have succeeded in defining the following loose consensus for some structural aspects of T cell recognition: that the germline-encoded complementarity-determining region 1 (CDR1) and CDR2 loops generally engage the helices of the MHC, whereas the hypervariable CDR3 loops have a more important function in engaging the peptide. Despite wide variation in the details of peptide recognition and in TCR-pMHC orientation geometry, the TCR 'polarity' over the pMHC surface is always such that the TCR variable α-chain (V_α) 'footprint' lies over the MHC class Ia α2-helices or MHC class II β-helices and peptide amino terminus, whereas the TCR V_β domain lies over the MHC class Ia α1-helices or MHC class II α-helices and the peptide carboxyl terminus[1].

One possible explanation for the invariant polarity could be that external constraints, such as the monomorphic coreceptors CD8 or CD4 or the invariant signaling protein CD3, impose specific steric requirements needed for the components of the complex to 'lock' together as a unit to form a productive signaling complex. This is unlikely, given the extremely wide variations in TCR-pMHC binding geometries, which would be difficult to explain if a common coreceptor interaction restricted the relative TCR-pMHC binding modes. In addition, complexes incorporating both coreceptor-dependent and coreceptor-independent TCRs, and both MHC class Ia and MHC class II molecules, share the same polarity[2]. These considerations indicate orientational freedom of or an absence of external restriction on the TCR-pMHC interaction.

An alternative explanation for the invariant polarity is an internal constraint; that is, an 'engrafted' mutual-recognition 'code' in germline TCR and MHC genes. The structural solution reported for TCR-MHC complexes so far is consistent with the idea that coevolution of genes encoding TCR V segments and MHC alleles resulted in germline-encoded elements in the TCR loci that are predisposed to bind to MHC molecules[3]. Abundant experimental evidence suggests that αβTCRs have a bias toward MHC recognition[4,5]. Kinetic measurements of TCR and pMHC have shown low-affinity interactions consistent with 'pan-MHC scanning' by the TCR[6,7]. One model proposes that TCRs and pMHC interact by a two-step mechanism whereby the MHC helices first weakly associate with CDR1 and CDR2 loops and the interaction is then stabilized and MHC-bound peptide is recognized mainly by CDR3 loops[8]. These immunological observations collectively give credence to the idea of a 'primordial' affinity between TCR and MHC driven by conserved sets of germline-encoded elements, which are then modulated by the MHC-bound peptide.

Given the limited repertoire of V genes and MHC molecules that have evolved together, an important issue is whether there are 'structural rules' dictating TCR-MHC interactions. Recognition 'codons' for specific MHC haplotypes and/or alleles and TCRs

[1]Howard Hughes Medical Institute, Department of Molecular & Cellular Physiology, Department of Structural Biology, Stanford University School of Medicine, Stanford, California 94305, USA. [2]Present address: Department of Chemical Engineering, University of Texas at Austin, Austin, Texas 78712, USA. Correspondence should be addressed to K.C.G. (kcgarcia@stanford.edu).

Received 14 May; accepted 17 July; published online 12 August 2007; doi:10.1038/ni1502

encoded by specific types of V-gene segments may restrict and define binding orientation. However, so far evidence for such a 'code' has not emerged from the structural database, as TCR-pMHC complexes do not seem to share obviously conserved, specific pairwise contact motifs composed of interacting residues on both the TCR and MHC. One explanation that has been proffered is that TCR-MHC interactions (such as those between CDR1 and CDR2 loops and MHC helices) are degenerate and are directed against shared structural determinants on the MHC helix backbone and not against particular amino acid side chains[9]. A further elaboration of that idea suggests that the specificity of the TCR-MHC interaction is derived in part from the absence of obstructive amino acids on the tops of the MHC helices that would interfere with the approach of TCR, rather than from the presence of specific sets of pairwise contacts[10]. The idea of 'specificity by omission' runs counter to prevailing ideas of protein-protein interactions. Even low-affinity 'promiscuous' interactions, such as might be imagined to underlie TCR-MHC recognition bias, are driven by exquisitely specific interatomic van der Waals and hydrogen bonds. Molecular recognition between proteins may be facilitated by, but is not driven by, the absence of inhibitory interactions; instead, recognition is driven by the presence of direct, specific bonding chemistries with small geometric tolerances. Thus, if the physical and chemical principles of TCR-MHC interactions are not different from those of other protein-protein interactions, the polarized TCR-MHC binding geometry would be expected to result from specific pairwise interactions that are evolutionarily conserved; this principle should be discernable from structural analysis.

It has been especially difficult to identify conserved amino acid interactions from sets of TCR-pMHC complexes with different TCR V segments, MHC haplotypes and unrelated peptides. Here we address this issue by focusing on a narrow 'slice' of the TCR repertoire, specifically the interaction of multiple TCRs encoded by a single germline element, V_β8.2, with a single MHC class II molecule, I-A^u. Our studies examine three well characterized TCRs derived from mice with experimental autoimmune encephalomyelitis, an intensively studied model system used to understand autoimmunity to neural self antigens such as myelin basic protein (MBP)[11]. The immunodominant encephalitogenic T cell epitope of MBP, recognized by T cells in mice of the H-2^u haplotype (PL/J or B10.PL), is the acetylated amino-terminal 11–amino acid sequence (MBP1-11)[12]. The T cell response to this epitope has been studied extensively[13]; it shows highly biased TCR V_β8.2-chain usage[14,15]. Salient correspondence of interatomic contacts has been reported between CDR1β and CDR2β loops and α-helices in crystal structures of the V_β8.2-containing 172.10 TCR bound to the I-A^u–MBP1-11 complex[16] and the V_β8.2-containing D10 TCR bound to the I-A^k–conalbumin complex[17]. We have also analyzed two more complexes of V_β8.2-containing TCRs bound to I-A^u–MBP1-11; the two TCRs have V_α segments, joining (J) segments and CDR3 sequences distinct from those of 172.10 and D10. However, these V_β8.2 TCR–I-A interactions also superimposed almost identically with those of the 172.10 and D10 complexes, and a mutational scan of the CDR1β and CDR2β loops of two different TCRs demonstrated identical 'energetic landscapes'. Thus, four TCR complexes show nearly identical interactions between CDR1β and CDR2β loops and I-A. We propose that this represents an initial 'proof-of-concept' for the existence of conserved pairwise interaction motifs, in effect 'codons', for recognition between particular TCR V_β segments and MHC haplotypes.

Table 1 V_β**8.2 TCRs recognizing I-A**

	1934.4	CI19	172.10	D10
$V_\alpha J_\alpha$	V_α4.1 J_αT31	V_α4.1 J_αT31	V_α2.3 J_α39	V_α2 J_α4
$V_\beta D_\beta J_\beta$	V_β8.2 D_β2.1 J_β2.3	V_β8.2 D_β2.1 J_β2.4	V_β8.2 D_β2.1 J_β2.7	V_β8.2 D_β1.1 J_β2.1
CDR3α	ALSENYGNEKI	ALSENYGNEKI	AASANSGTYQ	AATGSFNKL
CDR3β	ASGDASGAETL	ASGDASGGNTL	ASGDAGGYEQ	ASGGQGRAEQ
MHC-peptide	I-A^u–MBP1-11	I-A^u–MBP1-11	I-A^u–MBP1-11	I-A^k–conalbumin

RESULTS

Structural overview

The 1934.4 TCR[18] and cl19 TCR[19] both use V_α4.1 and V_β8.2 segments, but they use different J_β segments and CDR3β sequences (**Table 1**). In contrast, the 172.10 TCR[20] uses different V_α, J_β and CDR3β sequences. Thus, structures of the 1934.4, cl19 and 172.10 TCRs bound to the same pMHC complex provide three 'snapshots' of how differences in V_α, J_α, J_β, CDR3α and CDR3β sequences, when paired with a common Vβ8.2, influence recognition of the same pMHC complex (I-A^u–MBP1-11). The D10–I-A^k–conalbumin complex[17] affords the opportunity to compare how this common V_β8.2 element, paired with a distinct V_α segment, recognizes a unique pMHC complex in which the MHC is very similar to I-A^u but the peptides are entirely different. We expressed single-chain Fv fragment versions of 1934.4 and cl19, as well as a single-chain I-A^u–MBP1-11 construct, according to published methods and crystallized the TCR-pMHC complexes[16,21,22].

We determined the crystal structures of the 1934.4 and cl19 single-chain $V_\alpha V_\beta$ heterodimers in complex with I-A^u–MBP1-11 to resolutions of 2.2 Å and 2.7 Å, respectively (**Fig. 1** and **Table 2**). Both TCRs adopted the canonical binding orientation with the V_α domain poised over the amino terminus of the peptide and the V_β domain over the carboxy-terminal end of the peptide, resulting in an approximately diagonal docking orientation relative to the peptide and MHC helices[1]. As typically noted for TCR-pMHC structures, the complexes showed moderate shape complementarity, with values of 0.70 for the 1934.4 complex and 0.64 for the cl19 complex. The total buried surface areas at the TCR-pMHC interface were 2,060 $Å^2$ and 2,023 $Å^2$ for the 1934.4–I-A^u–MBP1-11 and cl19–I-A^u–MBP1-11 complexes, respectively, with approximately equal contribution from the TCR and pMHC subunits. For the TCRs, the V_α domain contributed

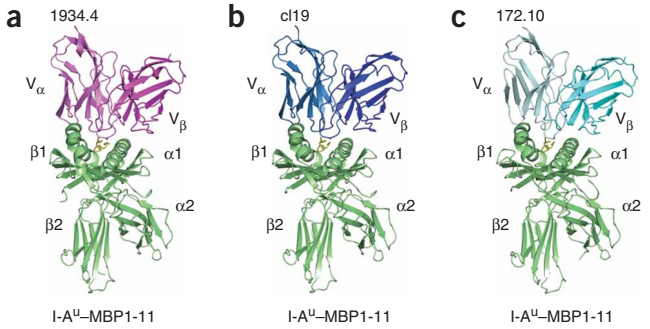

Figure 1 Structural overview of three experimental autoimmune encephalomyelitis–related TCRs in complex with I-A^u–MBP1-11. Crystal structures of 1934.4 and cl19 complexes were solved in this study; the crystal structure of the 172.10 complex has been reported before[16]. (**a**) The 1934.4–I-A^u–MBP1-11 complex: violet, V_α; magenta, V_β; green, I-A^u; yellow, MBP1-11. (**b**) The cl19–I-A^u–MBP1-11 complex: slate, V_α; blue, V_β. (**c**) The 172.10–I-A^u–MBP1-11 complex: pale cyan, V_α; dark cyan, V_β.

Table 2 Data collection and refinement statistics

	1934.4–I-A^u–MBP1-11	cl19–I-A^u–MBP1-11	Unbound 1934.4
Data collection			
Space group	$P4_122$	$P4_122$	I222
Cell dimensions (Å)	97.6; 97.6; 175.6	97.3; 97.3; 174.3	68.0; 73.8; 115.4
Resolution (Å)	47.0–2.2	97.0–2.7	50.0–2.2
Unique reflections	42,263	23,722	13,532
Redundancy[a]	4.3 (4.1)	10.5 (10.3)	6.0 (6.1)
Completeness (%)	100 (100)	99.8 (100)	96.1 (99.4)
$I/\sigma(I)$[a]	23.4 (3.5)	20.5 (2.7)	22.2 (5.6)
R_{merge}(%)[a]	10.3 (45.8)	9.2 (54.9)	6.6 (37.2)
Refinement statistics			
Resolution (Å)	47.0–2.2	50.0–2.7	50–2.2
R_{work} (%)[b]	21.5	23.5	26.3
R_{free} (%)[b]	25.3	28.7	28.5
r.m.s. deviation from ideality			
Bond lengths (Å)	0.006	0.008	0.007
Bond angles (°)	1.37	1.31	1.39
Ramachandran plot statistics			
Most favored (%)	89.2	88.1	80.3
Additionally allowed (%)	10.8	11.9	19.7
Generally allowed (%)	0	0	0
Disallowed (%)	0	0	0

Values in parentheses are for the shell of highest resolution.
[a]$R_{merge} = \Sigma|I_i - /I/_i$, where I_i is the intensity of an individual reflection and I is the average intensity of that reflection. [b]$R_{work} = \Sigma||F_o|-|F_c|/\Sigma|F_o|$. R_{free} is as for R_{work}, but calculated for a randomly selected 5.0% of reflections not included in the refinement.

approximately 60% of the buried surface area in both complexes. The peptide contribution to the pMHC buried surface area was 23% for the 1934.4 complex and 24% for the cl19 complex; these values are at the lower end of the range noted before for TCR-pMHC complexes[1].

As mentioned, 1934.4 and cl19 have the same V_α segments but differ in both J_β segments and CDR3β loops (**Table 1**). When we superimposed the two TCR-pMHC complexes on the I-A^u–MBP1-11 subunits (r.m.s. deviation, 0.34 Å^2), we noted that the TCRs had a similar binding footprint on the pMHC (**Fig. 2a**). This observation suggests that differences in CDR3β sequence are not manifest in differences in MHC footprints of the two TCRs. The relative conformations of the CDR loops were also very similar (**Fig. 2b**). The 1934.4 and cl19 footprints also superimposed closely with that reported before for 172.10 bound to I-A^u–MBP1-11 (ref. 16).

Diverse V_α-chain footprints

The CDR1α and CDR2α loops of 1934.4 and cl19 adopted very similar conformations and formed an overlapping network of bonds with the I-A^u β-chain helix (**Fig. 3**). Three residues from each of the CDR1α loop (Ser27, Gly28 and Tyr29) and CDR2α loop (Arg48, Ser50 and Arg51) on the TCR interface were involved in these interactions with the I-A^u β-chain helix region stretching from Arg70 to Tyr81 (**Supplementary Table 1** online). In both complexes, CDR1α Ser27 and CDR2α Arg51 formed hydrogen bonds with I-A^u Tyr81 and Asp76, respectively. Although the V_α footprints were nearly identical, there were some minor differences in atomic contacts made by CDR1α and CDR2α in the 1934.4 and cl19 complexes (**Supplementary Table 1**) that may reflect subtle differences or simply the different resolutions of the two complexes (2.2 Å and 2.7 Å).

The overall footprint of the 172.10 CDR1α and CDR2α loops was similar to the corresponding footprints for 1934.4 and cl19, but the interatomic contacts were distinct (**Fig. 3**). Whereas the cl19 and 1934.4 V_α domains formed many hydrogen bonds with MHC residues, the 172.10 V_α formed only van der Waals contacts with I-A^u. Six 172.10 CDR1α and CDR2α residues interacted with the same region of the I-A^u β-chain helix as cl19 and 1934.4, spanning I-A^u residues from Glu69 to Tyr81. In the CDR1α loop of 172.10, Ser27 and Ala28 interacted by van der Waals forces with Tyr81 of I-A^u, and Asp30 of the TCR interacted with Thr77 of I-A^u. These contacts were analogous to the corresponding Ser27, Gly28 and Tyr29 interactions made by 1934.4 and cl19. Whereas 1934.4 and cl19 formed an extensive network of CDR2α interactions through Arg48 and Arg51 (with I-A^u residues Arg70, Ala73 and Asp76), the 172.10 CDR2α loop contained small hydrophobic residues (Leu50 and Val52) that formed a single van der Waals contact each with I-A^u Glu69 and Ala73, respectively. Thus, although the location of the V_α domains over the MHC are similar, their respective bonding chemistries are distinct.

Conserved V_β8.2 recognition motifs

In contrast to the results reported above, 1934.4 and cl19 bound to I-A^u–MBP1-11 assumed V_β footprints over I-A^u identical to those of

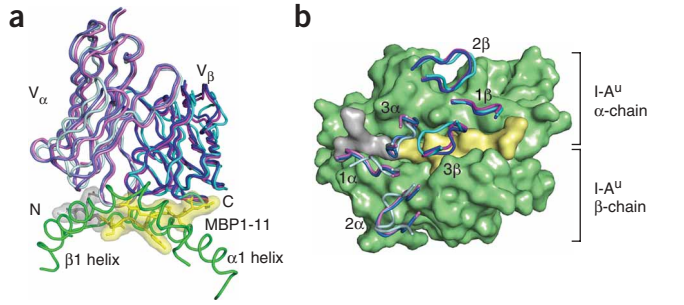

Figure 2 Superposition of 1934.4, cl19 and 172.10 complexes aligned on I-A^u–MBP1-11. Violet, 1934.4 V_α; magenta, 1934.4 V_β; slate, cl19 V_α; blue, cl19 V_β; pale cyan, 172.10 V_α; dark cyan, 172.10 V_β. (**a**) Side view of the complexes superimposed on the MHC. MBP1-11 is presented as a transparent (yellow) molecular surface with 'ball-and-stick' amino acids, including the remaining residues from the leader peptide (gray). The β-helix of I-A^u is in front and the α1-helix is behind the peptide. (**b**) Top view of the overlay of CDR footprints on the I-A^u–MBP1-11 composite surface.

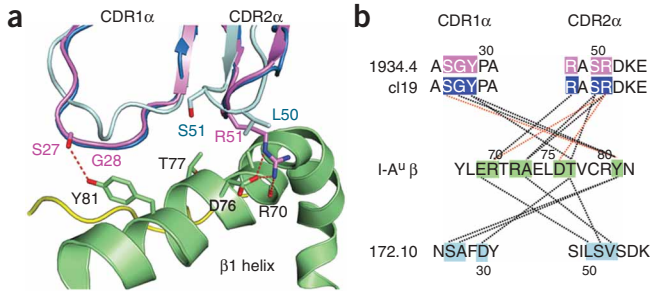

Figure 3 Heterogeneous interactions of CDR1α and CDR2α loops with the I-A^u β-helix. (**a**) Structures of 1934.4, cl19 and 172.10 from TCR-pMHC complexes superimposed on I-A^u (colors as in **Fig. 1**). Red dashed lines, hydrogen bonds. (**b**) Interactions between TCR CDR1α and CDR2α loops and the I-A β-helix. Highlighting indicates residues involved in interactions; black dashed lines, van der Waals forces; red dashed lines, hydrogen bonds. Top, interactions of 1934.4. Minor differences in interatomic contacts made by cl19 and 1934.4 are in **Supplementary Table 1**.

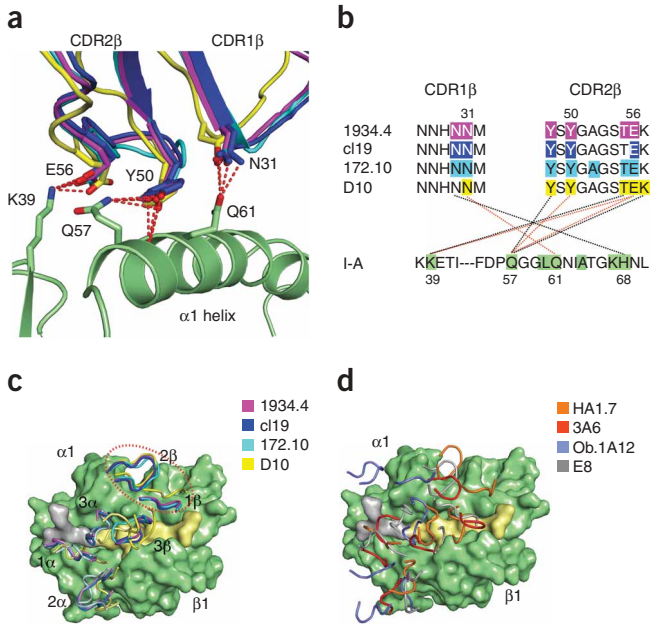

Figure 4 Recognition 'codon' between V_β8.2 and I-A. (**a**) Similar hydrogen-bonding network for four superimposed V_β8.2-containing TCR complexes with I-A (I-A^k from the D10 complex and I-A^u from the 1934.4, cl19 and 172.10 complexes): magenta, 1934.4; blue, cl19; cyan, 172.10; yellow, D10; red dashed lines, conserved hydrogen bonds between TCR CDR1β and CDR2β loops and the I-A α1-helix. (**b**) Shared interactions between the V_β8.2 CDR1 and CDR2 loops in **a** and the I-A α1-helix. Highlighting indicates all TCR and MHC residues involved in interactions; residues not highlighted are designated as contacts. I-A residues in green are conserved across various I-A allotypes (I-A^u, I-A^k, I-A^d, I-A^b, I-A^q, I-A^r and I-A^f). Red dashed lines, hydrogen bonds; black dashed lines, van der Waals interactions. For several TCR and MHC residues (such as D10 CDRβ Asn30), the assignment of hydrogen bond or van der Waals interaction is ambiguous because of the resolution differences of the structures; in such cases, the interaction is designated here as van der Waals. (**c**) Top view of the TCR CDR1β and CDR2β loop footprints (dashed red circle) on the pMHC composite surface. (**d**) Divergent footprints of other MHC class II–restricted TCRs aligned on I-A^u: the HA1.7 TCR footprint (orange) from the crystal structure of HA1.7 bound to HLA-DR1–HA (Protein Data Bank accession code, 1FYT); the 3A6 TCR footprint (red) from the crystal structure of 3A6 bound to HLA-DR2a–MBP87-99 (Protein Data Bank accession code, 1ZGL); the Ob.1A12 TCR footprint (slate) from the crystal structure of Ob.1A12 bound to HLA-DR2–MBP85-99 (Protein Data Bank accession code, 1YMM); and the E8 TCR footprint (gray) from the crystal structure of E8 bound to HLA-DR1–TPI (Protein Data Bank accession code, 2INA).

172.10 over I-A^u–MBP1-11 and D10 over I-A^k–conalbumin[16]. The 1934.4 and cl19 CDR1β and CDR2β loops had very similar positions and conformations (**Fig. 4a–c**) and formed a network of bonds with the I-A^u α-chain (**Fig. 4a,b**), suggesting a conserved recognition strategy for V_β8.2-encoded TCRs binding I-A MHC haplotypes (**Supplementary Table 1**). The convergence of the V_β8.2 footprints on I-A^u contrasts with the wide variation in docking modes seen in other human MHC class II–restricted TCR complexes (**Fig. 4d**). CDR1β Asn31 and CDR2β Tyr48, Tyr50 and Glu56 mediated interactions with the I-A^u α-helix in each of the structures (**Fig. 4a,b**). These four TCR residues interacted through both hydrogen bonds and van der Waals contacts with three α-chain residues conserved throughout all I-A MHC alleles (Lys39, Gln57 and Gln61)[16] (**Fig. 4b**). CDR2β Tyr50 is notable in that in all four complexes it formed a 'knob-in-hole' interaction with the I-A α-helix whereby the aromatic side chain lay flat and parallel to the helical axis, inserting between the Gln57 and Gln61 side chains (**Fig. 4a**).

The constellation of contacts between the V_β8.2 and I-A helix we found here was indeed mediated by amino acid side chains rather than being directed mainly by the MHC helix backbone. However, compared with other receptor-ligand interfaces, the TCR-MHC interfaces noted here were somewhat structurally unique and did encompass some features presciently suggested in published studies[9,10,23]. Side-chain interactions did not occur between the extended tips of residues on the α-helices and residues on the CDR loops. Instead, the CDR loops seemed to penetrate, or interdigitate, between side chains of the helix. The 'landing pads' on the MHC helices for both V_α and V_β CDR loops are devoid of large side chains, and steric inhibitions that would obstruct the close approach of a TCR. Such gaps in the α-helices may enable the CDR1 and CDR2 loops to bind in such a way as to allow maximum contact of the CDR3 loop with the MHC-bound peptide.

Peptide recognition mediated by main-chain contacts

As with the 172.10 TCR[16], interactions of the 1934.4 and cl19 TCRs with peptide were mediated entirely by the CDR3 loops, with no involvement of germline-encoded V_α and V_β residues. Also as with the 172.10 complex, most peptide contacts were not specific for 1934.4 and cl19 CDR3-loop side chains; in contrast, main-chain atoms of CDR3 loops engaged in interactions with peptide side chains (**Fig. 5**). That observation may be due at least in part to the presence of glycine residues at the tips of the CDR3α and CDR3β loops. The 1934.4

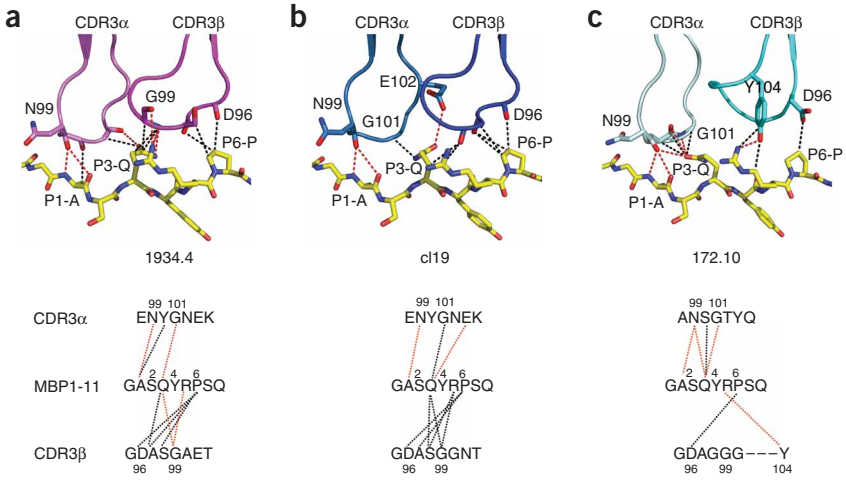

Figure 5 Main-chain interactions dominate contacts between TCR CDR3 loops and MBP1-11. Yellow, peptide; red dashed lines, hydrogen bonds; black dashed lines, van der Waals interactions. TCR amino acids are designated by one-letter amino acid code followed by position number; peptide amino acids are designated by position (P) number, followed by the one-letter amino acid code. Below, two-dimensional projections of the CDR3-peptide contacts. (**a**) The 1934.4 complex. (**b**) The cl19 complex. (**c**) The 172.10 complex.

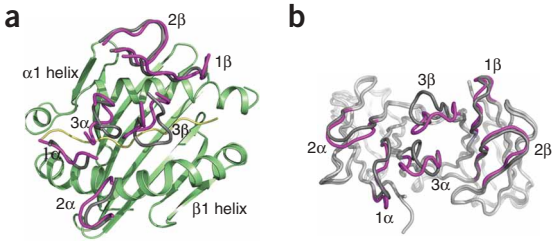

Figure 6 Large CDR3 conformational changes in the bound versus free structures of 1934.4. Light gray, 1934.4 V_α and V_β chains; green, I-A^u; yellow, MBP1-11; magenta, ligand-bound CDR loops; dark gray, non-ligand-bound CDR loops. (**a**) Top view. (**b**) View into the TCR combining sites.

CDR3β-loop main-chain atoms formed hydrogen bonds with the glycine residue at peptide position 3 (P3-Gln) and P5-Arg and formed van der Waals interactions with P3-Gln, P5-Arg and P6-Pro side chains. The 1934.4 CDR3α loop formed two main-chain hydrogen bonds with the peptide main chain (P1-Ala and P3-Gln) and van der Waals interactions with P1-Ala and P3-Gln side chains. Cl19 interacted with the same peptide residues but lacked the hydrogen bonds to P3-Gln and P5-Arg mediated by Gly99 of the 1934.4 CDR3β loop. This limited use of the full side-chain capability of the CDR3 loops to recognize the peptide is, to our knowledge, unique to these three TCR complexes (**Fig. 5** and **Supplementary Table 1**). Despite this apparent structural degeneracy, scans for peptides able to bind 172.10 TCRs showed an exquisite specificity for P3-Gln, P5-Arg and P6-Pro peptide side chains[16]. Thus, the 1934.4 and cl19 structures confirm that TCRs can be very specific in the face of main-chain interactions with peptide.

CDR3 loop conformational change after ligation

Given the apparent structural degeneracy of the CDR3-peptide interactions in this series of TCRs and the finding that four complexes assumed identical V_β8.2 domain–mediated interactions with I-A molecules, we investigated the function of CDR3 conformational plasticity in the binding of these TCRs to the pMHC complexes. To address this issue, we solved the crystal structure of one of the non-ligand-bound TCRs, the 1934.4 single-chain $V_\alpha V_\beta$ heterodimer, to a resolution of 2.2 Å (**Table 2**) and compared its CDR3 loop structure with that of the crystal structure of the same TCR bound to pMHC (**Fig. 6a**). Superposition of the non-ligand-bound and I-A^u–MBP1-11–bound 1934.4 TCRs showed similar global conformations (r.m.s. deviation, 1.21 $Å^2$). However, whereas the CDR1 and CDR2 loops underwent only minor conformational adjustments after pMHC ligation, the movement of the CDR3 loops was greater. The tip of the CDR3β loop moved 6.6 Å toward the peptide, such that Gly99 of CDR3β could form hydrogen bonds with peptide residues P3-Gln and P5-Arg. Although this movement would bring the two CDR3 loops in closer proximity, potential steric clashes were avoided, as the CDR3α loop moved toward the amino terminus of the peptide and underwent a conformational change to make contacts with P1-Ala and P3-Gln (**Fig. 6b**). The conformational changes noted in 1934.4 are consistent with the unfavorable binding entropy and anomalously large heat capacity measured before for this TCR-pMHC interaction and suggest that the CDR3 conformational change presents an energetic barrier to pMHC binding[24].

The conformational changes reported above suggest several conclusions. First, although the CDR3-peptide interactions seem to have a rather nonspecific structural chemistry in terms of pairwise amino acid contacts, there are strict conformational requirements for the recognition of peptide by a CDR3 loop. In particular, CDR3β of 1934.4 was 'bent' inward such that it buried the peptide surface area extending from peptide position 3 to position 5. This extensive surface coverage probably imposes specific shape complementarity requirements on the peptide that are 'read out' by CDR3. Second, the conserved network of interactions that constitute the V_β8.2–I-A interaction motif persisted despite the energetic cost and mechanical torque of the CDR3 conformational change during binding. Thus, in this case, the germline-encoded contacts seem to exert a slight energetic dominance relative to the adaptive, recombined elements of the TCR-pMHC interface.

Analysis of germline-encoded TCR-MHC contacts

It is possible that this conserved V_β8.2–I-A interaction motif is the structural manifestation of an innate, germline-encoded 'bias' of the TCR V_β8.2 domain for the I-A β-chain helix. If this were the case, we reasoned that the energetic footprint of V_β8.2 would likewise be conserved, whereas the energetic footprint of the different V_α domain–I-A interactions would be more heterogeneous. To test this hypothesis, we generated a series of alanine substitutions in CDR1 and CDR2 loops of 172.10 and 1934.4 and measured the contribution of each side chain to I-A binding by surface plasmon resonance (**Fig. 7** and **Supplementary Fig. 1** and **Supplementary Table 2** online). Alanine-scanning mutagenesis is a commonly used technique to measure the relative contributions of side-chain interactions to macromolecular interfaces[25]. This technique has been applied during the analysis of many TCR-pMHC interactions and has been used to make substitutions on both the TCR and MHC sides of the interfaces[8,26–29]. We used alanine-scanning mutagenesis but did not make CDR3 substitutions, as our goal was to assess the germline-encoded TCR-MHC contacts.

We assessed the footprints of 1934.4 and 172.10, as these TCRs have different V_α segments. Each bound to I-A^u–MBP1-11 with moderately

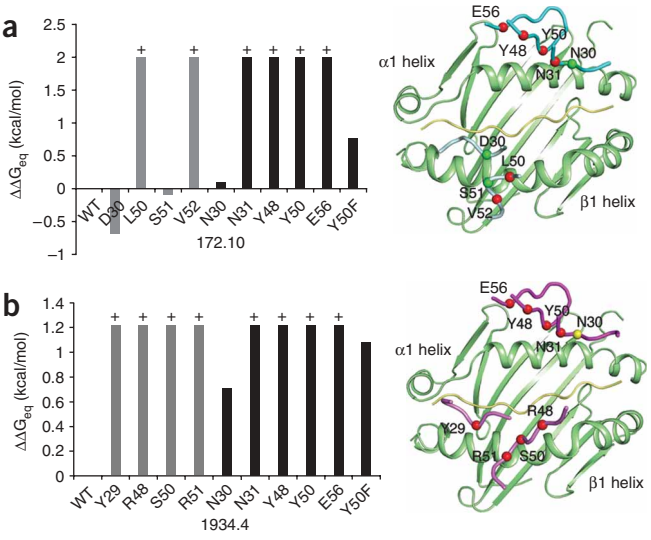

Figure 7 Effects of substitutions of CDR1 and CDR2 on the interactions of 1934.4 and 172.10 with IA^u–MBP1-11. Left, change in free energy ($\Delta\Delta G_{eq}$) associated with binding to I-A^u–MBP1-11 induced by substitutions (horizontal axes) in 172.10 (**a**) and 1934.4 (**b**). Gray bars, V_α mutants; black bars, V_β mutants; + (above bars), free energy changes of over 2.0 kcal/mol (**a**) or 1.2 kcal/mol (**b**). WT, wild-type. Right, maps of substituted amino acid residues on the structure of each TCR-pMHC complex. Colors indicate the energetic contribution (change in free energy) of the amino acid to TCR-pMHC binding: red, 1.2 kcal/mol or more; yellow, 0.6–1.2 kcal/mol; green, 0.6 kcal/mol or less.

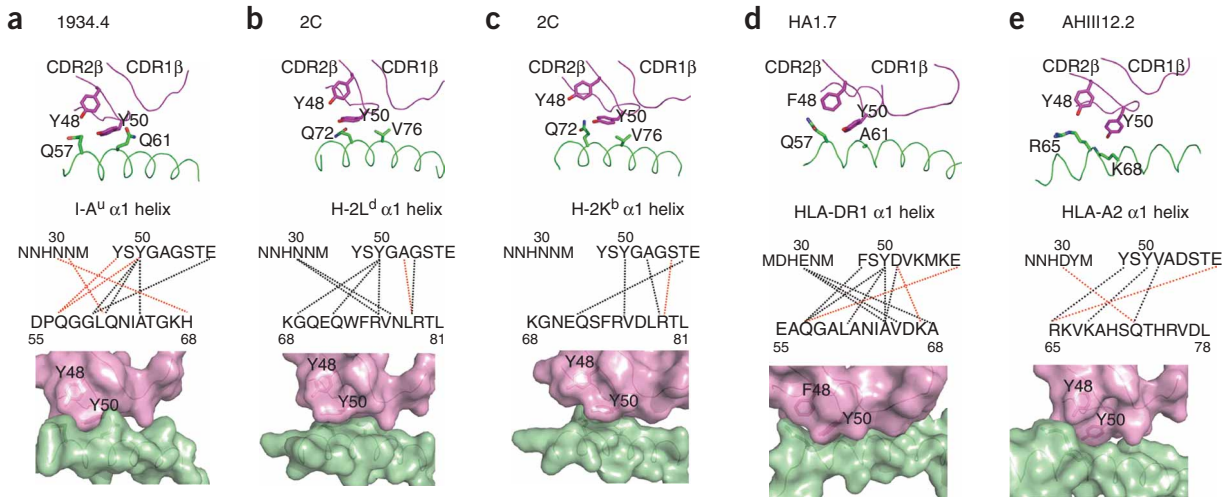

Figure 8 Recurrent involvement of aromatic residues in the CDR2β recognition strategy of different MHC class I and class II helices. CDR2β residues Tyr48 and Tyr50 are presented on five TCR-pMHC complexes. (**a**) 1934.4–I-A^u. (**b**) 2C–H-2L^d (ref. 30). (**c**) 2C–H-2K^b (ref. 23). (**d**) HA1.7–HLA–DR1 (ref. 31). (**e**) AHIII12.2–HLA–A2 (ref. 2). Top, interactions of Tyr48 and Tyr50 with MHC helices; middle, contact maps as primary sequences; bottom, surface representations of shape complementarity.

weak affinity (25.4 μM and 6.6 μM, respectively; **Supplementary Table 2b**). This weak affinity, reflected in slow 'on rates' and fast 'off rates', is characteristic of most TCR-pMHC interactions[7]. We chose residues for substitution in each of the CDR1 and CDR2 loops based on the side chain–mediated contacts seen in the complex structures (**Supplementary Table 2a** and **Supplementary Fig. 1**) and substituted nine residues in each TCR (four in V_α and five in V_β). In addition to the series of alanine substitutions, we substituted Tyr50 in each CDRβ chain with phenylalanine to gauge the relative contribution of the hydroxyl moiety versus the phenol ring at this position. As with the unsubstituted TCRs, all 20 substituted TCRs were soluble and were expressed at high yields with a periplasmic secretion construct[22]. All alanine mutants were monomeric on a S75 gel filtration column and eluted together at the same position as the unsubstituted TCR (data not shown).

The TCRα footprints were the most divergent energetic features of 172.10 versus 1934.4 (**Fig. 7**). Whereas each of the V_α CDR1 and CDR2 contacts between 1934.4 and I-A^u were critical, substitution of only two of the 172.10 V_α contacts resulted in substantial losses in binding free energy (**Supplementary Table 2b**). Given the sequence and structural differences, we could not make a strict residue-for-residue comparison, so we chose residues on CDR1α and CDR2α from each TCR that seemed structurally equivalent and important for pMHC binding, as indicated by hydrogen bonding, formation of van der Waals contacts and burial of surface area with I-A^u (**Fig. 3** and **Supplementary Fig. 1**). Asp30 of 172.10 formed two van der Waals interactions with Thr77 of the I-A^u β-chain; however, substitution of Asp30 with alanine increased the affinity of the TCR-pMHC by –0.7 kcal/mol (**Fig. 7**), presumably due to a fourfold increase in the association rate (**Supplementary Table 2b**). Thus, Asp30 may slightly impede TCR-pMHC association through electrostatic repulsion. In contrast, substitution of Tyr29 of 1934.4 with alanine, which made comparable contacts with the MHC helix by packing between Thr77 and Tyr81, with the aromatic ring making van der Waals contacts with Thr77, completely abrogated TCR-pMHC binding. The increase in packing interactions mediated by Tyr29 relative to Asp30 is concordant with a greater energetic contribution of Tyr29 (**Supplementary Table 2b**).

For 172.10, the contribution of CDR2α involved the packing of Leu50, Ser51 and Val52 (**Fig. 3** and **Supplementary Fig. 1**). Substitution of Leu50 or Val52 with alanine removed favorable van der Waals interactions and completely abrogated binding (**Fig. 7** and **Supplementary Table 2b**). In contrast, substitution of Ser51 with alanine had only a slight effect on affinity, indicating that the hydroxyl group is probably not important. CDR2 of 1934.4 packed against a similar region along the I-A^u β-chain helix as that of 172.10 did; however, the loop conformation of 1934.4 CDR2α is more extended, allowing for more side-chain contacts. The extended loop structure and greater number of contacts correlated with a greater energetic contribution for 1934.4 CDR2 than for 172.10, as substitution of any of the 1934.4 CDR2 residues completely abolished pMHC binding.

In contrast, and consistent with the observed structural similarities, the relative 'energetic landscapes' for V_β interactions between pMHC and both 172.10 and 1934.4 were nearly identical (**Fig. 7** and **Supplementary Table 2b**). Only two of eight residues in CDR1β (Asn30 and Asn31) directly contacted I-A^u. Of these, Asn30 imparted the only moderately large energetic difference between 172.10 and 1934.4. The basis of this energetic difference is not apparent from the crystal structures. In both structures, Asn30 forms side chain–mediated van der Waals bonds with His68 of I-A^u, and the extent of this interaction is nearly identical for the two structures.

The conserved energetic footprint of CDR2β for 172.10 and 1934.4 was the most salient feature of all the V_β8.2 structures. For both 172.10 and 1934.4, Tyr48, Tyr50, and Glu56 formed a dense hydrogen-bonding network with I-A^u residues Gln57, Lys39, and Gln61. This resulted in 'knob-in-hole' packing of Tyr50 into a cleft on the top of the α-helix of I-A^u formed by the gap between Gln57, Leu60 and Gln61 (**Fig. 4** and **Supplementary Fig. 1**). Glu56 of the TCR formed a hydrogen bond with Lys39 and Asn57 of I-A^u. This oriented Gln57 of I-A^u, allowing a hydrogen bond to form between the amide nitrogen and the hydroxyl oxygen of CDR2β Tyr48, which stacked against the aromatic ring of CDR2β Tyr50. Substitution of Tyr48, Tyr50 or Glu56 with alanine eliminated TCR-pMHC binding, supporting the conclusion that each residue is crucial for the energetics of TCR-pMHC complex formation (**Supplementary Table 2**).

We sought to determine whether this 'knob-in-hole' packing (**Fig. 8a**) of the Tyr50 phenol ring was uniquely important in the MHC interface. This was of particular interest because Tyr50 also made a hydrogen bond between the side-chain hydroxyl group and a main-chain carboxyl group. To study this, we also substituted Tyr50 with phenylalanine. Both the hydroxyl group and the phenol ring were crucial for binding, and the alanine substitution had a greater effect than the phenylalanine substitution (**Fig. 7**). The phenylalanine substitution in 172.10 reduced the binding energy by 0.77 kcal/mol and resulted in a slightly slower 'on rate' and a faster 'off rate'. The corresponding substitution in 1934.4 was more notable, as it caused a drop of 1.18 kcal/mol in the binding energy. From these results, it is difficult to assess the extent to which this hydrogen bond acts to properly orient the phenol ring to allow efficient packing against the MHC α-helix.

Our alanine-scanning analysis demonstrated that the V_β8.2 domain has a common energetic footprint in the two TCR-pMHC complexes that is specific to the amino acid side chain (**Fig. 7**). This strengthens the argument for the existence of a conserved, pairwise V_β-pMHC interaction motif. However, the contribution of V_α cannot be ignored, as these contacts remain energetically critical in both complexes, albeit to different degrees.

Generality of the CDR2β strategy for recognition of MHC

In the four V_β8.2–I-A complex structures, both Tyr48 and Tyr50 were in similar conformations, with Tyr50 oriented parallel to the MHC α-helix and packed into a depression between side chains on the $I\text{-}A^u$ α-helix (**Fig. 8a**). We found that similar conformations of these TCR residues were also present in CDR2β of the V_β8.2-containing 2C–H2-K^b structure (**Fig. 8b**) and 2C–H2-L^d structure (refs. 28,30; **Fig. 8c**), although these two complexes do not accommodate Tyr50 with such 'knob-in-hole' complementarity or form the same amino acid side-chain helix contacts as the V_β8.2–I-A complexes. Notably, analysis of human and mouse V_β regions has shown tyrosine to be the most common residue used at positions 48 and 50 (43% and 28% of all mouse and human V_β regions, respectively). Of the TCR-pMHC complex structures solved so far, both AHIII12.2–HLA-A2 (Vβ8.1)[2] (**Fig. 8d**) and HA1.7–HLA-DR1 (Vβ31.1)[31] (**Fig. 8e**) have a tyrosine residue at position 50. AHIII12.2 also has a tyrosine at position 48, whereas HA1.7 has a phenylalanine, which is aromatic, in this position. In both cases, these two aromatic residues (at positions 48 and 50) are used to contact the MHC helix[2,31], with the CDR2β loop of AHIII12.2 adopting an interaction mode very similar to that noted for the Vβ8.2 TCRs. Assignment of the CDR2β-MHC motifs noted here (**Fig. 8b–e**) as 'codons' will depend on the persistence of these contacts in additional TCR-pMHC complex structures sharing these V_β and related alleles of MHC. Thus, the chemical and conformational flexibility of aromatic residues on CDR2β seems to be exploited by the TCR to form multifarious yet specific contacts with a spectrum of MHC helical surfaces.

DISCUSSION

Here we have presented structural and mutational data supporting the idea that TCRs containing a particular germline-encoded element, V_β8.2, form amino acid–specific, conserved interactions with the helical residues of I-A. Our observations emphasize the idea that sets of TCR-MHC interaction motifs, in effect 'codons' of MHC restriction, arose through coevolution. The addition of two more V_β8.2 TCR-pMHC complexes to the pre-existing set of 172.10 TCR–pMHC complexes[16] and D10 TCR–pMHC complexes[17] further confirms that hypothesis, which has been suggested by biological data but so far has remained unsubstantiated by structural data. These results collectively represent a systematic analysis of interactions between a single TCR V domain with a highly related subset of MHC molecules.

Our study sheds light on the invariant orientational polarity of TCRs bound to MHC molecules. In each of the complexes analyzed here, the V_β8.2–I-A interactions persisted even though the V_α domains differed. Thus, it is likely that the V_β 'codon' determined, or at least strongly influenced, the rotational orientation. This interpretation is in accordance with the V_β8.2 bias noted in TCRs derived from the experimental autoimmune encephalomyelitis system[15]. These TCR complexes may be 'V_β-centric', whereas TCRs derived from other systems may be 'V_α-centric', meaning that the TCR orientation and polarity may be dictated by a V_α 'codon'. However, the idea of a 'V_β-centric' TCR is not meant to imply an energetically inert V_α chain. That was not the case here, as many V_α substitutions were still detrimental to V_β8.2 TCR–pMHC binding, albeit to substantially different degrees than for V_β and to substantially different degrees for distinct V_β8.2 TCR–pMHC complexes.

If MHC bias is dictated by evolutionarily conserved recognition motifs, or 'codons', then the observed polarity in all known TCR-pMHC structures is probably a reflection of either selection for V_α segments that recognize the α2- and β-helices of MHC, selection of V_β segments that recognize the α1- and α-helices of MHC, or both. Given the generally random pairing of TCRα and TCRβ, the variable effect each chain-pairing combination may have on MHC binding chemistry and the extreme diversity of antigenic peptides that could 'edit' or influence the binding geometry of each TCR-pMHC interaction, we speculate that each V segment may encode several possible structural 'codons' that can be used when binding a particular MHC. As seen in the KB5-C20–pBM1–H-$2K^b$ and BM3.3–VSV8–H-$2K^b$ complexes[32,33], a given V_β domain has several possible 'landing spots' on a given MHC helix and probably 'chooses' which to use according to the V_α it associates with or the peptide it contacts. However, an important principle is that the number of 'codons' is probably finite, given that V-domain–MHC contacts evolved together with a mutual specificity.

In principle, a table could be constructed of TCR-MHC interaction 'codons' that define the contacts between each V segment and each MHC haplotype or allele. Conceptually, compilation of this list could begin by study of a particular V_α or V_β segment paired with a range of V_β or V_α segments, respectively, and comparison of the binding of each pair to the same MHC haplotype presenting both common and unique peptides. To some extent, a few of these structures are available in the present TCR-pMHC structural database. The A6 and B7 TCRs both share a common V_β12.3 segment, and complex structures are available for both bound to HLA-A2–Tax[34,35]. Notably, these crystal structures show a common V-segment footprint. However, it is not in the shared V_β segment; in contrast, it involves the V_α chain, specifically homologous residues at the tip of CDR2α. The structures of KB5-C20–VSV8–H-$2K^b$, and BM3.3–pBM1–H-$2K^b$, both of which share a common V_β2 segment[32,33], have few shared V_β contacts. This is probably because of differences between the antigenic peptide (VSV8 for KB5-C20 and pBM1 for BM3.3). The 'blurring' of the interaction motifs in these complexes makes it apparent that for the 'codons' to emerge most distinctly, it will be important to hold all components of the interacting partners (V genes, MHC alleles and peptides) constant, or at least similar, while varying one V segment at a time.

Several V_β8.2-containing TCR structures have been determined in complex with different MHC–peptide complexes[23,30], but such similarities in binding have not been reported. One reason that we

'visualized' this particular V_β8.2–I-A 'codon' with such clarity in these TCRs may be that the CDR3-peptide interactions were structurally degenerate in nature and were dominated by main-chain interactions from CDR3; there was no contact of CDR1 or CDR2 with peptide. This relative dearth of side-chain interactions and competing influences of CDR1 and CDR2 may have resulted in a minimum of peptide-mediated 'editing' of the TCR footprint on the MHC. Data obtained with TCR–peptide–MHC class I complexes involving the same TCR and the same MHC but structurally distinct peptides have shown that subsections of a conserved, optimal $V_\alpha V_\beta$ 'landing spot' can be reused to adapt to nonoptimal peptides[36]. That is, different peptides probably influence a TCR to use one of several possible binding 'codons' that result in binding affinities and kinetics optimal for peptide recognition, scanning and/or TCR signaling. The MBP-specific TCRs may have converged on a low-energy 'codon' relatively unperturbed by peptide. It has been noted from the initial structures of I-A–peptide complexes how structurally degenerate the peptide sequences are, with a preponderance of small side chains[16]. When the peptide is more prominent or bulged, V-domain contacts may have less of a effect on influencing orientation[37]. Certainly there are examples in which TCR-peptide energetic contacts 'trump' any innate bias in either the V_β or V_α chain[29,38].

The elements of the MHC restriction 'codon' for V_β8.2 TCRs described here may reflect more fundamental rules governing the association of proteins. The observation that Tyr48 and Tyr50 of CDR2β had similar conformations in different V_β complexes is reminiscent of the canonical conformations of CDRs in antibodies[39] and the 'preferential' use of specific amino acids, most notably tyrosine and serine, in antibody combining sites[40]. It has been speculated that the bias toward tyrosine and serine in antibodies reflects the chemical flexibility inherent in these residues and their ability to make productive associations with both polar and aliphatic residues. That idea is supported by the results of a series of phage-display experiments in which antibodies of high affinity and specificity for many protein antigens were generated in which the CDR amino acid composition was limited to tyrosine and serine[41]. The V_β8.2 'codon' described here may exploit that same chemical flexibility to allow productive associations with multiple MHC molecules. Studies have noted the similarity between CDR conformations in TCRs and canonical conformations of antibody CDRs[42]. CDR2β of V_β8.2 was reported to be most similar to the α2-3 conformation of CDR2 in antibody heavy chains. Thus, in a way similar to antibodies, germline-encoded TCR CDR loops may have evolved a chemical and conformational optimum to satisfy the opposing requirements of specific but cross-reactive recognition of a diverse spectrum of MHC surfaces.

METHODS

Protein preparation. MHC class II molecule I-A^u, with MBP1-11 attached to the amino terminus of the β1 domain, was expressed and purified as described[21]. The stabilized (4Y) version of the peptide, which binds I-A^u with high affinity because of burial of the 4Y MHC anchor but is recognized by TCRs in a way identical to recognition of the wild-type peptide, was expressed. Three residues from the artificial leader peptide remained at the amino terminus of the peptide after secretion and were visible in the electron density map[21]. The 1934.4 TCR construct design, protein expression and purification initially followed the same strategy used for the 172.10 TCR[22]. Crystals for non-ligand-bound 1934.4 diffracted to a resolution of 2.2 Å; however, large single crystals of the 1934.4 complex diffracted to a resolution of only 7–8 Å. To improve the resolution, two modifications were made to the 1934.4 expression construct. First, the three residues located at the carboxyl terminus of the V_α domain, Thr-Ile-Lys, were substituted with Gln-Val-Val, the counterpart sequence of 172.10. This modification eliminated potential crystal packing 'clashes' that may have been induced by the long side chain of lysine residue. Second, the histidine tag was moved from the carboxyl terminus of V_β domain to the amino terminus of the V_α domain, and a tobacco etch virus protease site was included between the histidine tag and the amino-terminal residue of the protein. Protein was extracted by osmotic shock and was purified by sequential immobilized metal affinity, anion exchange and S75 size-exclusion chromatographic steps. The amino-terminal histidine tag was removed by overnight digestion at 4 °C with a 1:100 mass ratio of tobacco etch virus protease before size exclusion. These two modifications were also engineered into the cl19 TCR construct.

Crystallization. All crystals were grown at 22 °C by the 'sitting-drop' technique with a ratio of 1:1 for protein/reservoir drop. Large single crystals of unbound 1934.4 single-chain TCR were grown from 1934.4 (30 mg/ml) in 0.8 M monosodium dihydrogen phosphate, 0.8 M mono-potassium dihydrogen phosphate and 0.1 M HEPES, pH 7.5. For the TCR-pMHC complexes, a 1:1 molar ratio of TCR-pMHC was mixed at a concentration of 20 mg/ml. Large single crystals of both 1934.4 and cl19 complexes grew in 0.2 M potassium sodium tartrate tetrahydrate, 0.1 M succinic acid, pH 7.0, and 16% (wt/vol) polyethylene glycol 3350.

Data collection, structure determination and refinement. All data sets were collected at beamline 11-1 at the Stanford Synchrotron Radiation Laboratory. Data were indexed, integrated and scaled with HKL2000 software[43]. Non-ligand-bound 1934.4 was 'cryo-cooled' in the presence of 15% (wt/vol) ethylene glycol in reservoir buffer. The structure was determined by molecular replacement with the MOLREP program (CCP4 suite)[44] with the α-chain of 1934.4 (ref. 45) and the β-chain of 172.10 (ref. 16) as the search models. The structure was then built with COOT software[46] followed by refinement with the crystallography and nuclear magnetic resonance system[47]. For the 1934.4 complex, the crystal was 'cryo-cooled' in reservoir buffer plus 15% (wt/vol) glycerol and a data set at 2.2 Å was collected. The 1934.4 complex was solved by molecular replacement with the PHASER program[48], with 1934.4 and the binary I-A^u–MBP1-11 complex[21] as the search models. The structure was built with COOT software followed by refinement with the crystallography and nuclear magnetic resonance system. The molecular graphics program PyMol[49] was used to make the structure figures.

Surface plasmon resonance. The affinity and kinetics of the binding of soluble single-chain TCRs and variants to I-A^u–MBP1-11 were analyzed by surface plasmon resonance. I-A^u–MBP1-11 was expressed with a carboxy-terminal BirA peptide from baculovirus-infected Hi Five cells (Invitrogen) by published methods[24]. Approximately 800 and 2,000 resonance units of biotin-tagged I-A^u were captured on the surface of a BIAcore SA chip preimmobilized with streptavidin. Single-chain TCRs or variants were injected for 60 s at various concentrations in the range of 1–200 μM. The complex was allowed to dissociate for 1 min between injections. The background response was measured by simultaneous injection over a control surface containing immobilized nonclassical MHC molecule T22, and these values were subtracted to yield the binding response. BIAevaluation (Version 3.0; BIAcore), assuming a 1:1 Langmuir binding model, was used for all data fitting.

Accession codes. Protein Data Bank: 2PXY, 2Z31 and 2Z35.

Note: Supplementary information is available on the Nature Immunology website.

ACKNOWLEDGMENTS

We acknowledge M. Davis for discussions and access to a BIAcore 3000. Supported by the National Institutes of Health (AI48540 to K.C.G.), the Howard Hughes Medical Institute (K.C.G.) and the National Health and Medical Research Council of Australia (CJ Martin Fellowship to L.K.E.).

AUTHOR CONTRIBUTIONS

D.F., X-ray crystallographic analyses; D.F., C.J.B, L.K.E. and J.M., biochemical and biophysical studies; and K.C.G., project direction.

COMPETING INTERESTS STATEMENT

The authors declare no competing financial interests.

Published online at http://www.nature.com/natureimmunology
Reprints and permissions information is available online at http://npg.nature.com/reprintsandpermissions

1. Rudolph, M.G., Stanfield, R.L. & Wilson, I.A. How TCRs bind MHCs, peptides, and coreceptors. *Annu. Rev. Immunol.* **24**, 419–466 (2006).
2. Buslepp, J., Wang, H., Biddison, W.E., Appella, E. & Collins, E.J. A correlation between TCR V_α docking on MHC and CD8 dependence: implications for T cell selection. *Immunity* **19**, 595–606 (2003).
3. Jerne, N.K. The somatic generation of immune recognition. *Eur. J. Immunol.* **1**, 1–9 (1971).
4. Blackman, M. *et al.* The T cell repertoire may be biased in favor of MHC recognition. *Cell* **47**, 349–357 (1986).
5. Zerrahn, J., Held, W. & Raulet, D.H. The MHC reactivity of the T cell repertoire prior to positive and negative selection. *Cell* **88**, 627–636 (1997).
6. Matsui, K. *et al.* Low affinity interaction of peptide-MHC complexes with T cell receptors. *Science* **254**, 1788–1791 (1991).
7. Krogsgaard, M. & Davis, M.M. How T cells 'see' antigen. *Nat. Immunol.* **6**, 239–245 (2005).
8. Wu, L.C., Tuot, D.S., Lyons, D.S., Garcia, K.C. & Davis, M.M. Two-step binding mechanism for T-cell receptor recognition of peptide MHC. *Nature* **418**, 552–556 (2002).
9. Huseby, E.S. *et al.* How the T cell repertoire becomes peptide and MHC specific. *Cell* **122**, 247–260 (2005).
10. Huseby, E.S., Crawford, F., White, J., Marrack, P. & Kappler, J.W. Interface-disrupting amino acids establish specificity between T cell receptors and complexes of major histocompatibility complex and peptide. *Nat. Immunol.* **7**, 1191–1199 (2006).
11. Zamvil, S.S. & Steinman, L. The T lymphocyte in experimental allergic encephalomyelitis. *Annu. Rev. Immunol.* **8**, 579–621 (1990).
12. Zamvil, S.S. *et al.* T cell specificity for class II (I-A) and the encephalitogenic N- terminal epitope of the autoantigen myelin basic protein. *J. Immunol.* **139**, 1075–1079 (1987).
13. Goverman, J. Tolerance and autoimmunity in TCR transgenic mice specific for myelin basic protein. *Immunol. Rev.* **169**, 147–159 (1999).
14. Acha-Orbea, H. *et al.* Limited heterogeneity of T cell receptors from lymphocytes mediating autoimmune encephalomyelitis allows specific immune intervention. *Cell* **54**, 263–273 (1988).
15. Urban, J.L. *et al.* Restricted use of T cell receptor V genes in murine autoimmune encephalomyelitis raises possibilities for antibody therapy. *Cell* **54**, 577–592 (1988).
16. Maynard, J. *et al.* Structure of an autoimmune T cell receptor complexed with class II peptide-MHC: insights into MHC bias and antigen specificity. *Immunity* **22**, 81–92 (2005).
17. Reinherz, E.L. *et al.* The crystal structure of a T cell receptor in complex with peptide and MHC class II. *Science* **286**, 1913–1921 (1999).
18. Pearson, C.I., van Ewijk, W. & McDevitt, H.O. Induction of apoptosis and T helper 2 (Th2) responses correlates with peptide affinity for the major histocompatibility complex in self- reactive T cell receptor transgenic mice. *J. Exp. Med.* **185**, 583–599 (1997).
19. Lafaille, J.J., Nagashima, K., Katsuki, M. & Tonegawa, S. High incidence of spontaneous autoimmune encephalomyelitis in immunodeficient anti-myelin basic protein T cell receptor transgenic mice. *Cell* **78**, 399–408 (1994).
20. Goverman, J. *et al.* Transgenic mice that express a myelin basic protein-specific T cell receptor develop spontaneous autoimmunity. *Cell* **72**, 551–560 (1993).
21. He, X.L. *et al.* Structural snapshot of aberrant antigen presentation linked to autoimmunity: the immunodominant epitope of MBP complexed with $I\text{-}A^u$. *Immunity* **17**, 83–94 (2002).
22. Maynard, J. *et al.* High-level bacterial secretion of single-chain αβ T-cell receptors. *J. Immunol. Methods* **306**, 51–67 (2005).
23. Garcia, K.C. *et al.* Structural basis of plasticity in T cell receptor recognition of a self peptide-MHC antigen. *Science* **279**, 1166–1172 (1998).
24. Garcia, K.C., Radu, C.G., Ho, J., Ober, R.J. & Ward, E.S. Kinetics and thermodynamics of T cell receptor-autoantigen interactions in murine experimental autoimmune encephalomyelitis. *Proc. Natl. Acad. Sci. USA* **98**, 6818–6823 (2001).
25. Cunningham, B.C. & Wells, J.A. High-resolution epitope mapping of hGH-receptor interactions by alanine-scanning mutagenesis. *Science* **244**, 1081–1085 (1989).
26. Manning, T.C. *et al.* Alanine scanning mutagenesis of an αβ T cell receptor: mapping the energy of antigen recognition. *Immunity* **8**, 413–425 (1998).
27. Lee, P.U., Churchill, H.R., Daniels, M., Jameson, S.C. & Kranz, D.M. Role of 2CT cell receptor residues in the binding of self- and allo-major histocompatibility complexes. *J. Exp. Med.* **191**, 1355–1364 (2000).
28. Baker, B.M., Turner, R.V., Gagnon, S.J., Wiley, D.C. & Biddison, W.E. Identification of a crucial energetic footprint on the alpha1 helix of human histocompatibility leukocyte antigen (HLA)-A2 that provides functional interactions for recognition by tax peptide/HLA-A2-specific T cell receptors. *J. Exp. Med.* **193**, 551–562 (2001).
29. Borg, N.A. *et al.* The CDR3 regions of an immunodominant T cell receptor dictate the 'energetic landscape' of peptide-MHC recognition. *Nat. Immunol.* **6**, 171–180 (2005).
30. Colf, L.A. *et al.* How a single T cell receptor recognizes both self and foreign MHC. *Cell* **129**, 135–146 (2007).
31. Hennecke, J., Carfi, A. & Wiley, D.C. Structure of a covalently stabilized complex of a human αβ T-cell receptor, influenza HA peptide and MHC class II molecule, HLA-DR1. *EMBO J.* **19**, 5611–5624 (2000).
32. Reiser, J.B. *et al.* Crystal structure of a T cell receptor bound to an allogeneic MHC molecule. *Nat. Immunol.* **1**, 291–297 (2000).
33. Reiser, J.B. *et al.* A T cell receptor CDR3β loop undergoes conformational changes of unprecedented magnitude upon binding to a peptide/MHC class I complex. *Immunity* **16**, 345–354 (2002).
34. Garboczi, D.N. *et al.* Structure of the complex between human T-cell receptor, viral peptide and HLA-A2. *Nature* **384**, 134–141 (1996).
35. Ding, Y.H. *et al.* Two human T cell receptors bind in a similar diagonal mode to the HLA-A2/Tax peptide complex using different TCR amino acids. *Immunity* **8**, 403–411 (1998).
36. Mazza, C. *et al.* How much can a T-cell antigen receptor adapt to structurally distinct antigenic peptides? *EMBO J.* **26**, 1972–1983 (2007).
37. Tynan, F.E. *et al.* T cell receptor recognition of a 'super-bulged' major histocompatibility complex class I–bound peptide. *Nat. Immunol.* **6**, 1114–1122 (2005).
38. Kjer-Nielsen, L. *et al.* A structural basis for the selection of dominant alphabeta T cell receptors in antiviral immunity. *Immunity* **18**, 53–64 (2003).
39. Chothia, C. & Lesk, A.M. Canonical structures for the hypervariable regions of immunoglobulins. *J. Mol. Biol.* **196**, 901–917 (1987).
40. Mian, I.S., Bradwell, A.R. & Olson, A.J. Structure, function and properties of antibody binding sites. *J. Mol. Biol.* **217**, 133–151 (1991).
41. Fellouse, F.A. *et al.* Molecular recognition by a binary code. *J. Mol. Biol.* **348**, 1153–1162 (2005).
42. Al-Lazikani, B., Lesk, A.M. & Chothia, C. Canonical structures for the hypervariable regions of T cell αβ receptors. *J. Mol. Biol.* **295**, 979–995 (2000).
43. Otwinowski, Z., Minor, W. & Carter, C.W., Jr. in *Methods in Enzymology* Vol. 276 (eds. Abelson, J.N., Simon, M.I., Carter, C.W. Jr. & Sweet, R.M.) 307–326 (Academic, New York, 1997).
44. Vagin, A. & Teplyakov, A. MOLREP: an automated program for molecular replacement. *J. Appl. Crystallogr.* **30**, 1022–1025 (1997).
45. Li, H., Lebedeva, M.I., Ward, E.S. & Mariuzza, R.A. Dual conformations of a T cell receptor V_α homodimer: implications for variability in $V_\alpha V_\beta$ domain association. *J. Mol. Biol.* **269**, 385–394 (1997).
46. Emsley, P. & Cowtan, K. COOT: model-building tools for molecular graphics. *Acta Crystallogr. D Biol. Crystallogr.* **60**, 2126–2132 (2004).
47. Brunger, A.T. *et al.* Crystallography & NMR system: A new software suite for macromolecular structure determination. *Acta Crystallogr. D Biol. Crystallogr.* **54**, 905–921 (1998).
48. Read, R. Pushing the boundaries of molecular replacement with maximum likelihood. *Acta Crystallographica D Biol. Crystallogr.* **57**, 1373–1382 (2001).
49. DeLano, W.L. The PyMol molecular graphics system. (DeLano Scientific, San Carlos, California, 2002).